Efficiency Analysis of a Sliding-Mode Controlled Quadratic Boost Converter

Oswaldo López-Santos is with the Methods and Algorithms in Control at the Laboratory for Analysis and Architecture of Systems, LAAS-CNRS, Toulouse, France; also with the Department of Electronic Engineering from Ibagué University, Ibagué, Colombia (e-mail: oswaldo.lopez@unibague.edu.co).

Luis Martínez-Salamero is with the Department of Electrical, Electronic and Control Engineering from Rovira i Virgili University, Tarragona, Spain (e-mail: luis.martinez@urv.cat).

Germain García is with the Methods and Algorithms in Control at the Laboratory for Analysis and Architecture of Systems, LAAS-CNRS, Toulouse, France. (e-mail: garcia@laas.fr).

Hugo Valderrama-Blavi is with the Department of Electrical, Electronic and Control Engineering from Rovira i Virgili University, Tarragona, Spain (e-mail: hugo.valderrama@urv.cat).

Daniel O. Mercuri is with HT S.A. Fuentes de Energía, Buenos Aires, Argentina (e-mail: danielmercuri@hotmail.com).

Abstract— A quadratic boost converter with high DC gain to step up the voltage of a standard photovoltaic panel up to 400 V is analyzed in this paper. First of all, a comparative analysis among boost, quadratic boost and cubic boost reveals that the quadratic boost exhibits the best trade-off between duty ratio range and converter efficiency. A hysteretic comparator is employed as a modulator to ensure the converter operation with high values of the duty ratio without risk of modulation saturation. A two-loop sliding –mode control is used to regulate the output voltage. An internal loop controls cycle by cycle the input current whose reference is established by an outer loop that processes the output voltage error by

means of a proportional-integral (PI) compensating network. Measured results in a 100 W prototype operating in continuous conduction mode (CCM) of average values, ripples, frequency and efficiency for different equilibrium points are in good agreement with the theoretical predictions.

Index Terms—DC-DC switching converters, quadratic boost, sliding-mode control, photovoltaic applications, and efficiency analysis.

1. INTRODUCTION

The market of grid-connected solar inverters has undergone a dramatic increase in the last years due to the liberalization of the electricity market in many countries and the implementation of government policies establishing interesting purchase prices for the electricity produced by means of renewable energies. Grid-connected inverters supply either 110 or 220 Vrms at 60 or 50 Hz respectively in one-phase or three-phase structures and can be classified into four categories, namely, micro, string, multi-string and central inverters. Micro-inverters are one–phase DC-AC converters operating with an input voltage range V_{in} between 25 and 50 V DC, and delivering an active power value not bigger than 300W. String inverters are also one-phase conversion structures with an input voltage in the range 40 to 200VDC, and an output power in the interval between 1 and 3 KW. Multi-string inverters can be indistinctly one- phase or three-phase circuits with input voltages between 50 and 600VDC and output power between 3 and 20KW.Finally, a central inverter is always a three-phase DC-AC converter supplying more than 20KW for an input voltage in the region 200-300VDC.

Grid connected solar micro-inverters consist basically of two stages, i.e. a first stage operating at high frequency to step up the panel voltage up to 400VDC and a second stage operating at the grid frequency to perform properly the transformation DC-AC and the subsequent connection to the public utility. Since they operate in the lowest power range, their weight and volume are susceptible of minimization in view of a mechanical integration in the back side of the same PV panel. However, the requirements for an optimal architecture in terms of power density, efficiency and the mentioned weight and volume lead more often than not to the formulation of a difficult problem whose solution is still open.

In our approach, a first step in the pursuing of minimization would be the absence of a high-frequency transformer, which is a common element to the most relevant commercial micro-inverters [1]. A second step could be defining the lowest input voltage in order to establish the maximum DC gain required by the voltage step-up converter. Hence, the next step would consist in finding potential converters without galvanic isolation that could solve the voltage step-up problem and subsequently select the most appropriate one by means of a comparative analysis.

The main goal of the work here reported is to demonstrate that a quadratic boost converter [2] is a competitive transformer-less structure to solve the problem of step-up an input voltage in the range 15-·30 V DC up to 400V DC. To solve this problem with only one switch-controlled circuit, it has been disregarded the use of cascade converters because it implies the use of two or more switches with their corresponding controllers [3]. It has been also neglected the use of converters with coupled inductors [4] - [5] due to the high voltage spikes produced by the leakage inductance across the power switch. Switched-capacitor –based power converters have not been taken into account because they are also used in cascade with a classical converter stage what makes the resulting converter very complex [6] . On the other hand, buck-boost, Cuk and SEPIC converters have been also rejected because they show smaller efficiency than the boost converter [7]. Therefore, solving the abovementioned problem of voltage step-up implies to select a candidate among a boost converter and its successive generalizations with only one controlled switch , namely, the quadratic boost converter and the cubic boost converter [2], [8].

It is expected that designing a voltage step up transformer-less single stage with a maximum DC gain of 20 will require duty cycle values near the unity with the risk of saturating the modulator. This analysis is carried out in section 2, where a comparison on equal basis among boost, quadratic boost and cubic boost is performed. The introduction of a hysteresis comparator in the regulation loop in order to guarantee the converter operation with high duty cycles without risk of modulator saturation leads to the sliding-mode control approach described in section 3 [9]. In the same section, it is also shown experimentally the dependence of the switching frequency on the coordinates of the equilibrium point. A Matlab –based analysis program is used in section 4 to predict the converter efficiency as a function of input voltage and output load, which are contrasted with experimental measurements in the same section. The conclusions and a discussion on the continuation of the work are presented in section 5.

2. SINGLE-SWITCH TOPOLOGIES BASED ON BOOST CONVERTER

Among the switching converters with a capability to supply an output voltage higher than the input one, the boost converter has been traditionally preferred due to its high-efficiency and the advantages associated to the fact that the controlled switch shares the same electrical reference with both input and output voltages. However, it is also well-known that the use of the boost converter for industrial applications is constrained to voltage gains less than 10 [10]. Hence, converters derived of the boost converter with gains higher than 10 have recently generated a great interest, especially in photovoltaic and fuel-cell applications [8], [11]. The circuit diagram of some of these power structures, named quadratic and cubic boost, is presented in figure 1 together with the one corresponding to the classical boost converter.

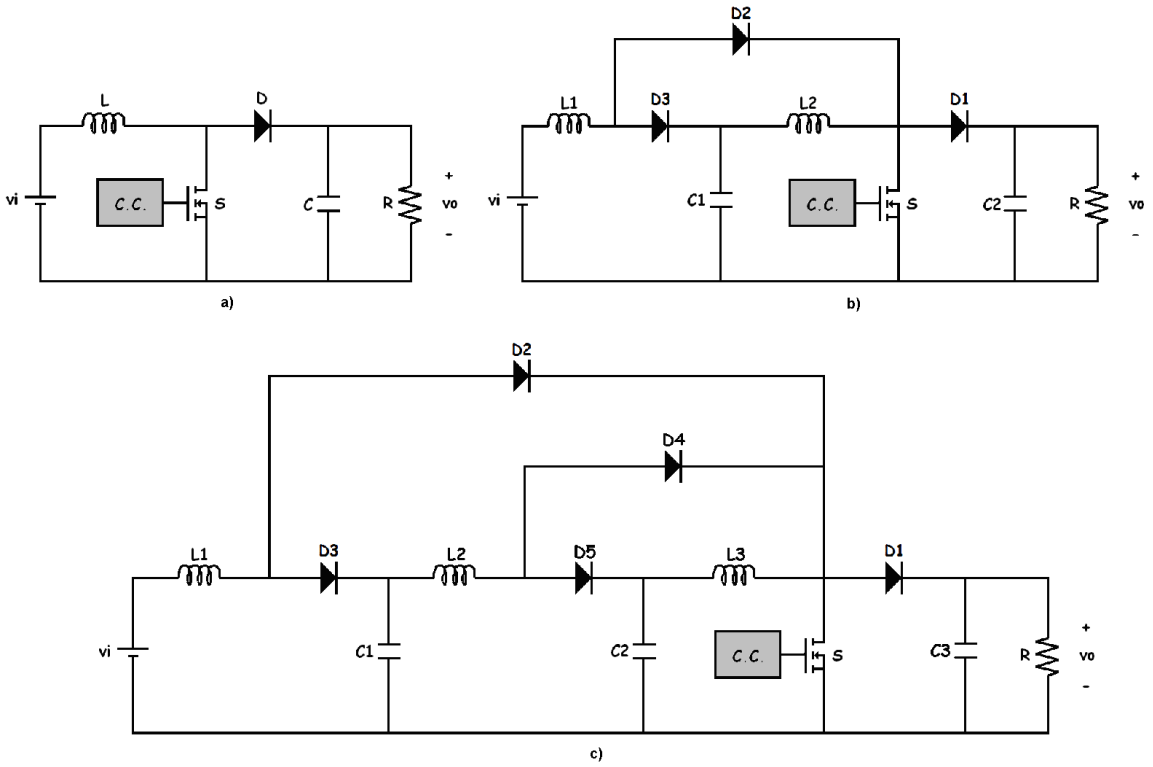

Fig. 1. Power circuit diagram: a) boost converter, b) quadratic boost, c) cubic boost.

The steady-state models of the configurations based in the boost converter have been generalized by Ortiz-Lopez et al. [8], so that the quadratic boost converter and the cubic boost converter correspond to the configurations with two and three stages respectively. Each stage has two passive elements i.e. one inductor and one capacitor, and in consequence the system order is a multiple of two. Similarly, two additional diodes are included to operate as complementary switches allowing the converter control with the same switch of the first stage. The main advantage of a multiple stage boost converter with respect to the classical boost stage is the possibility to obtain a higher gain with an inferior duty cycle and avoid saturation in the control signal. Nevertheless, as a consequence of the increase of the number of elements, these high order converters can result in both a reduction of efficiency and a growth of weight, size and price.

A relatively accurate model of the power converter operating in CCM can be obtained with the introduction of the resistive components of inductors, capacitors and power semiconductors. Although efficiency studies commonly employ models including only the equivalent series inductor resistance (ESL) as a main parasitic element because it affects both ON and OFF states of the controller switch, it can be expected that the introduction of other resistive elements would result in a better accuracy of the theoretical prediction of the model, what would eventually constitute a useful tool for a comparative analysis among power converters. Hence, in the analysis here reported it is also included both the equivalent series resistance in capacitors (ESR) and the ON-state resistance of the MOSFET, the diodes in the conduction state being represented with a voltage source and a series resistance.

In steady-state operation, the converter variables converge and remain in an equilibrium point for each unchanged parameter condition. Thus, the voltage-seconds balance in inductors and the charge balance in capacitors are applied to obtain the mean values of capacitor voltages and inductor currents in the equilibrium point [10]. Each storage energy element has an associated equation and the complete system can be solved as the linear equation $A \cdot x = B$. This solution can be analysed for a fixed load in the input voltage range to derive the DC gain behaviour as a function of the duty cycle. This procedure is applied in this section in order to obtain a graphic representation of the steady-state output voltage and output power as a function of the duty cycle for the boost converter, quadratic boost converter and cubic boost converter.

A. Boost converter steady-state model

In figure 2 a), when the controlled switch is in ON-state, the diode is already open and the inductor takes energy from the input power supply. At the same time, the output capacitor gives the energy to the load. In figure 2 b), when the controlled switch is in OFF-state, the diode is closed and the inductor

charges the output capacitor and gives the energy demanded by the load. Thus, the converter operates continuously between ON and OFF states. The equation system representation is given by (1).

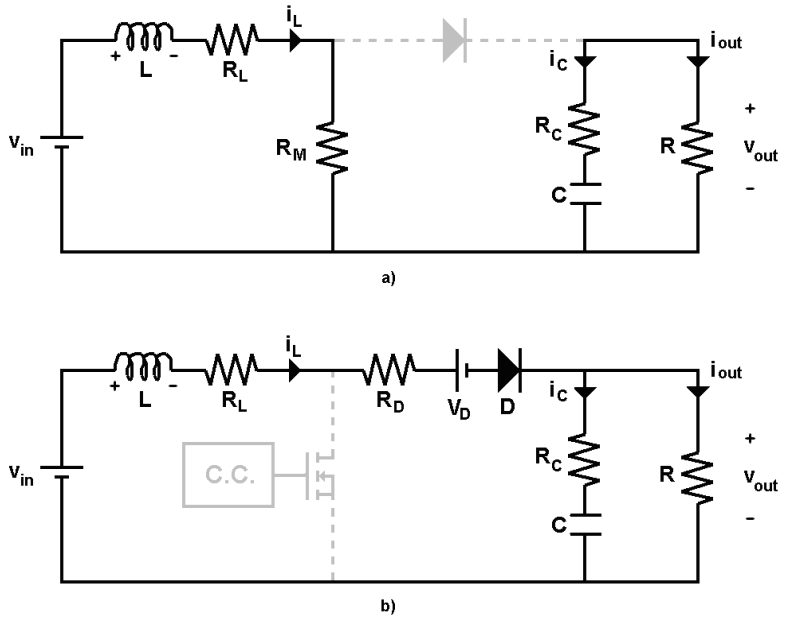

Fig. 2. Circuit configurations of a boost converter: a) ON state, b) OFF state.

$$\begin{bmatrix} R_L + R_M D + (R_D + R_C K_{out})D' & K_{out}D' \\ RD' & -1 \end{bmatrix} \begin{bmatrix} \mathrm{I_L} \\ \mathrm{V_C} \end{bmatrix} = \begin{bmatrix} V_{in} - V_D D' \\ 0 \end{bmatrix} \tag{1}$$

where $K_{out} = R(R + R_C)^{-1}$, $D' = 1 - D$ and $D = \frac{T_{ON}}{T}$ is the steady-state duty cycle.

Hence, solving V_C in (1) results in

$$V_C = \frac{RD'(V_{in} - D'V_D)}{R_L + R_M - D'R_M + D'R_D + D'R_C K_{out} + R(D')^2 K_{out}} \tag{2}$$

In the ideal case $K_{out} = 1$, all resistances are zero except R and $V_D = 0$, what implies

$$\frac{V_C}{V_{in}} = \frac{1}{D'} \qquad (3)$$

B. Quadratic boost converter steady-state model

In figure 3 a), when the controlled switch is in ON-state, diodes D1 and D3 are open and diode D2 is closed, inductor L1 takes energy from the input power supply and inductor L2 takes energy from capacitor C1. At the same time, output capacitor C2 gives the energy to the load. In figure 3 b), when the controlled switch is in OFF-state, diodes D1 and D3 are closed and diode D2 is open, inductors L1 and L2 charge capacitors C1 y C2 and give the energy demanded by the load. Therefore, the converter operates continuously between ON and OFF states. The equation system representation is given by (4).

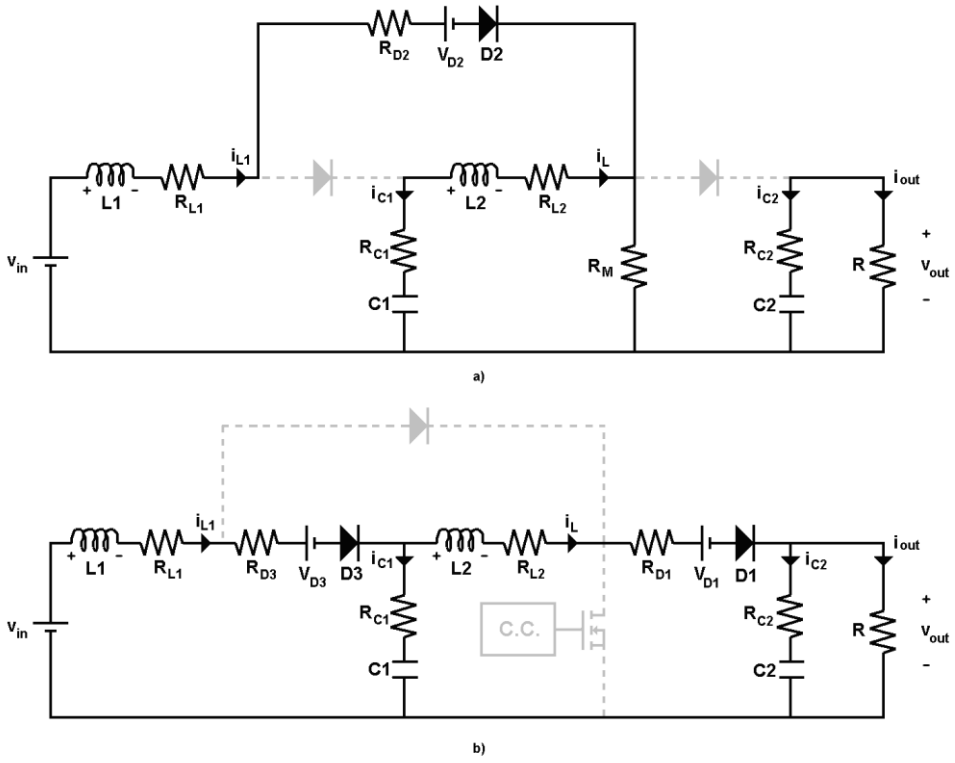

Fig. 3. Circuit configurations of a quadratic boost converter: a) ON state, b) OFF state.

$$\begin{bmatrix} R_{L1}+R_aD+R_bD' & R_MD-R_{C1}D' & D' & 0 \\ R_MD-R_{C1}D' & R_{L2}+R_{C1}+R_MD+R_eD' & -1 & K_{out}D' \\ D' & -1 & 0 & 0 \\ 0 & RD' & 0 & -1 \end{bmatrix} \begin{bmatrix} I_{L1} \\ I_{L2} \\ V_{C1} \\ V_{C2} \end{bmatrix} = \begin{bmatrix} V_{in}-V_{D2}D-V_{D3}D' \\ -V_{D1}D' \\ 0 \\ 0 \end{bmatrix} \quad (4)$$

where $R_a = R_M + R_{D2}$, $R_b = R_{D3} + R_{C1}$, $K_{out} = R(R+R_{C2})^{-1}$ and $R_e = R_{D1} + K_{out}R_{C2}$.

Hence, solving V_{C2} in (4) leads to

$$V_{C2} = \frac{R(D')^2\left[V_{in} + (D'-1)V_{D_2} - D'V_{D_3} - (D')^2V_{D_1}\right]}{R_a + R_{L1} - (D')^2R_{C_1} + (D')^2R_{L_2} + 2D'R_M - D'R_a + D'R_b + (D')^3R_e - (D')^2(1+D')R_M + R(D')^4K_{out}}$$

(5)

In the ideal case $K_{out} = 1$, all resistances are zero except R and $V_{D_i\,(i=1,..3)} = 0$, what implies

$$\frac{V_{C_2}}{V_{in}} = \frac{1}{(D')^2} \qquad (6)$$

C. Cubic converter steady-state model

In figure 4 a), when the controlled switch is in ON-state, diodes D1, D3 and D5 are open and diodes D2 and D4 are closed, inductor L1 takes energy from the input power supply, whereas inductor L2 takes energy from capacitor C1 and inductor L3 takes energy from capacitor C2 .At the same time, output capacitor C3 gives energy to the load. In Figure 4 b), when the controlled switch is in OFF-state, diodes D1 and D3 are closed and diode D2 is open, inductors L1, L2 and L3 charge capacitors C1, C2 and C3. Simultaneously, inductor L3 delivers the energy demanded by the load. Hence, the converter operates continuously between ON and OFF states. The equation system representation is given by (7).

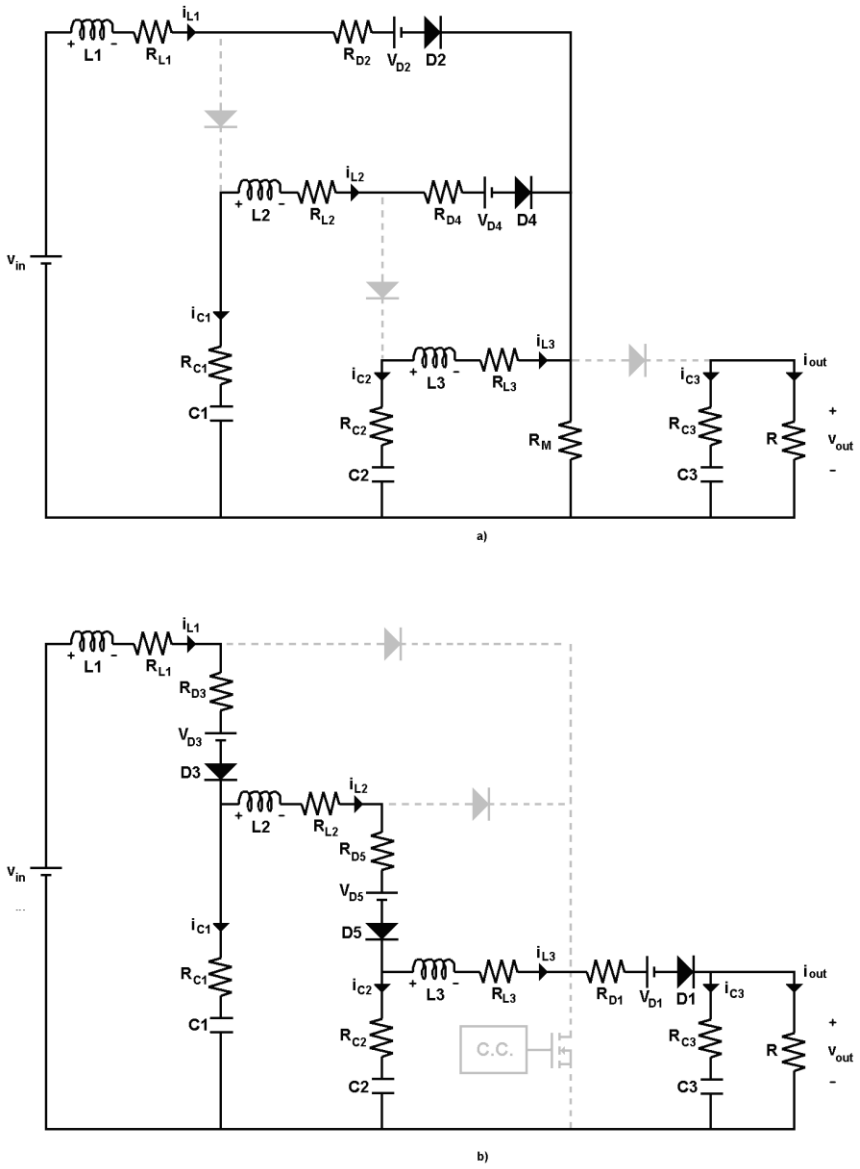

Fig. 4. Circuit configurations of a cubic boost converter: a) ON state, b) OFF state.

$$\begin{bmatrix} R_{L1}+R_aD+R_bD' & R_MD-R_{C1}D' & R_MD & D' & 0 & 0 \\ R_MD-R_{C1}D' & R_e+R_fD+R_gD' & R_MD-R_{C2}D' & -1 & D' & 0 \\ R_MD & R_MD-R_{C2}D' & R_h+R_MD+R_iD' & 0 & -1 & K_{out}D' \\ D' & -1 & 0 & 0 & 0 & 0 \\ 0 & D' & -1 & 0 & 0 & 0 \\ 0 & 0 & RD' & 0 & 0 & -1 \end{bmatrix} \begin{bmatrix} I_{L1} \\ I_{L2} \\ I_{L3} \\ V_{C1} \\ V_{C2} \\ V_{C3} \end{bmatrix} = \begin{bmatrix} V_{in}-V_{D2}D-V_{D3}D' \\ -V_{D4}D-V_{D5}D' \\ -V_{D1}D \\ 0 \\ 0 \\ 0 \end{bmatrix} \quad (7)$$

where $R_a = R_M + R_{D2}$, $R_b = R_{D3} + R_{C1}$, $R_e = R_{L2} + R_{C1}$, $R_f = R_{D4} + R_M$, $R_g = R_{D5} + R_{C2}$, $R_h = R_{L3} + R_{C2}$, $K_{out} = R\left(R + R_{C3}\right)^{-1}$ and $R_i = R_{D1} + K_{out} R_{C3}$.

Therefore, solving V_{C3} in (7) yields

$$V_{C3} = \frac{R(D')^3\left[V_{in} - (D')^3 V_{D_1} + (D'-1)V_{D_2} - D'V_{D_3} - D'(1-D')V_{D_4} - (D')^2 V_{D_5}\right]}{\begin{aligned} &R_a + R_{L1} - 2(D')^2 R_{C_1} - 2(D')^4 R_{C_2} + 2D'R_M - D'R_a + D'R_b + (D')^2 R_e - (D')^4 R_M - (D')^5 R_M \\ &+ (D')^2(1-D')R_f + (D')^3 R_g + (D')^4 R_h + (D')^5 R_i + R(D')^6 K_{out} \end{aligned}}$$

(8)

In the ideal case $K_{out} = 1$, all resistances are zero except R and $V_{D_i\,(i=1,..4)} = 0$, what implies

$$\frac{V_{C_3}}{V_{in}} = \frac{1}{(D')^3} \qquad (9)$$

D. Voltage gain and output power comparison

Using the values of parameters in Table 1 to evaluate voltage gain and output power in the previous converters, and assuming unregulated operation with a load resistance of 1600Ω lead to the output characteristics presented in figure 5 and figure 6, respectively. The references into brackets in Table I correspond to the semiconductor device employed subsequently in the experiments.

Table 1. Values of parasitic elements

Element	Value
$R_{L_i\,(i=1..3)}$	20mΩ
$R_{C_i\,(i=1..3)}$	40mΩ
R_M (STW45NM50)	80mΩ
$R_{Di\,(i=1..5)}$ (MUR860)	100mΩ
$V_{Di\,(i=1..5)}$ (MUR860)	0.52 V

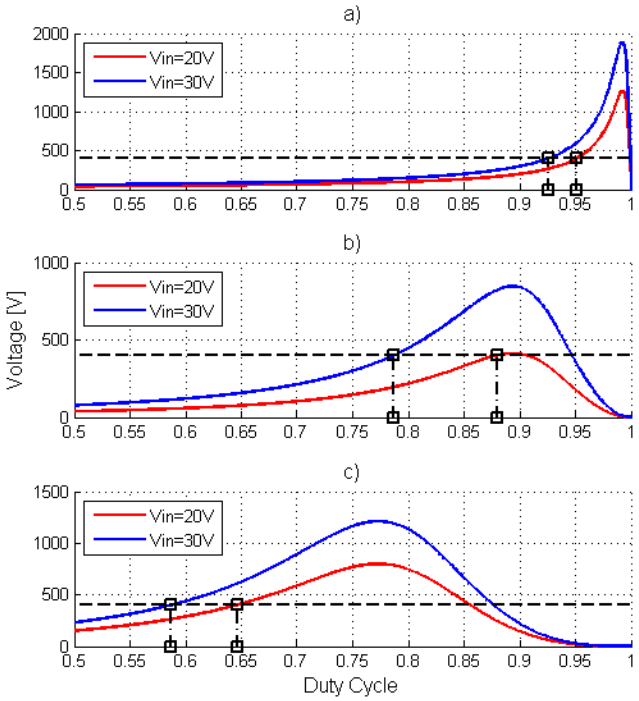

Fig. 5. Output voltage vs. duty cycle: a) boost, b) quadratic boost, c) cubic boost.

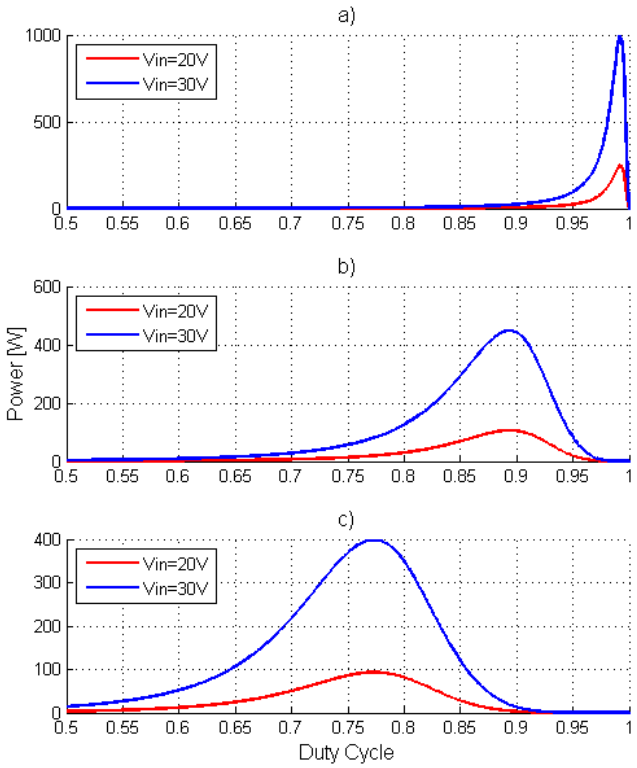

Fig. 6. Output power vs. duty cycle: a) boost, b) quadratic boost, c) cubic boost.

It has to be pointed out that the boost converter needs a duty cycle in the range between 92.0% and 95.0% to obtain the desired output voltage of 400V with an input voltage in the region between 20V and 30V, which is a reduced region that ensures a safe converter operation. In the quadratic boost converter, the duty cycle range is higher than that of the boost converter and it extends from 78.0% to 87.7%. This is an advantage because the sensitivity of the converter duty cycle to external disturbances is reduced. The cubic boost converter in turn must operate in a duty cycle range between 58.5% and 64.5%, which results in an operation area without risk of modulator saturation.

Moreover, based on the output power characteristics with fixed resistive load, it is easy to observe that the boost converter could lead to higher power levels than both quadratic and cubic solutions because its topology has fewer components and therefore better efficiency. However, in order to attain high power levels, the converter must operate in a non-safe area what precludes its use in industrial applications. The quadratic boost converter and the cubic boost converter can exhibit similar maximum power levels, but the efficiency in the cubic boost converter is inferior due to a higher number of components.

To summarize, it can be concluded that the required voltage gain in the DC-DC stage of grid connected solar micro-inverters can be obtained with the three studied converters. However, the boost quadratic converter presents the best trade-off between efficiency and risk of modulator saturation. Hence, the study of efficiency here reported is focused on the quadratic boost converter and takes into account special conditions of sliding-mode operation.

3. SLIDING-MODE CONTROLLED QUADRATIC BOOST CONVERTER

Including an inner current loop in the voltage regulation system of the DC-DC converters reduces the order of its dynamics. In addition, the effect of the non-minimum phase zeros present in the boost converter derived topologies is also reduced [12]. This concept has been applied to the quadratic boost converter with the approach of the current-mode control [13]. Therefore, taking into account the aforementioned advantages, we propose the control scheme shown in figure 7 where the current loop corresponds to a sliding mode- based controller. It can be observed that the inner loop consists in a hysteresis comparator that allows reaching a sliding surface defined by the input inductor current by providing the appropriate signals of activation and deactivation to the controlled switch. The outer loop compares the measured signal of the output voltage with the desired value so that the resulting error modifies the current reference in the inner loop by means of a PI compensator. Thus, expression (10) defines the control surface considering both inner and outer loops.

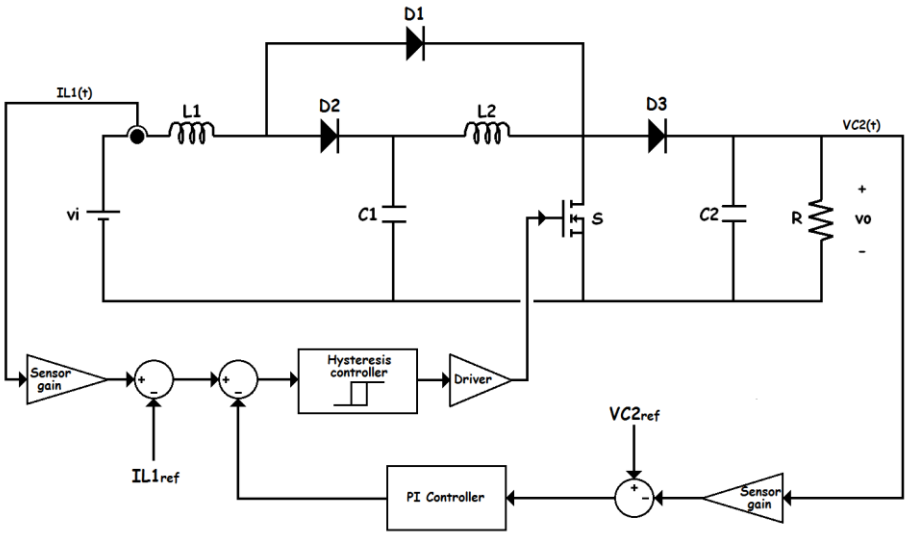

Fig. 7. Proposed control scheme of the sliding-mode based control with output voltage regulation.

$$S(x) = I_{L1ref} - I_{L1}(t) - K_p\left(V_{C2}(t) - V_{C2ref}\right) - K_i \int_{-\infty}^{t} \left(V_{C2}(t) - V_{C2ref}\right) dt \tag{10}$$

The steady-state analysis of DC-DC converters in CCM is basically the same for a control system based on either pulse width modulation (PWM) or hysteretic-band comparison. However, with controllers based on PWM, the converter operates with a fixed frequency for all parameter conditions, in a clear- cut contrast with the hysteresis comparator, wherein the switching frequency is a function of both input voltage and output power. Thus, different equilibrium points have different switching periods because of the variation of the corresponding ON and OFF times. Figure 8 illustrates the frequency change in the inductor current with a constant hysteresis band when the converter operates in two different equilibrium points which correspond to two different values of input voltage and the same value of output load.

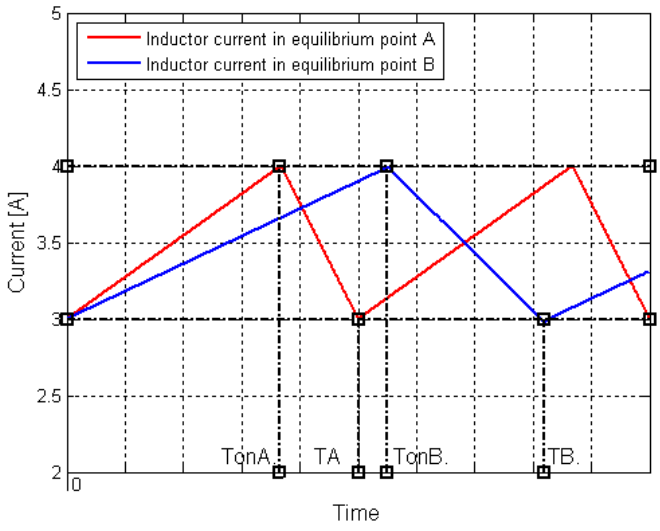

Fig. 8. Change of the switching frequency in sliding-mode operation.

The quantification of the frequency variation in the aforementioned control configuration requires studying the current ripple in the input inductor with the converter operating in an equilibrium point. Hence, it is worth obtaining independently the differential equations for the two positions in the controlled switch. In the ideal case, the expressions are as follows:

$$\frac{di_{L1}}{dt} = \frac{v_{in}}{L_1} \qquad \textit{with controlled switch in ON state} \tag{11}$$

$$\frac{di_{L1}}{dt} = \frac{v_{in}}{L_1} - \frac{v_{C1}}{L_1} \qquad \textit{with controlled switch in OFF state} \tag{12}$$

In expressions (11) and (12), we impose the limitation of the inductor current evolving linearly within the hysteresis band +/- δ around the steady-state average value. Thus, t_{ON} and t_{OFF} are defined by expressions (13) and (14) respectively.

$$t_{ON} = \frac{2L_1\delta}{V_{in}} \tag{13}$$

$$t_{OFF} = \frac{2L_1\delta}{V_{C1} - V_{in}} \tag{14}$$

where V_{C1} is the average value of capacitor voltage v_{C1} in steady-state.

The switching frequency f_s of the quadratic boost converter operating in sliding-mode is defined by the expression (15) where we have considered the steady-state value of the voltage V_{C1}.

$$f_s = \frac{1}{T_s} = \frac{1}{t_{ON} + t_{OFF}} = \frac{V_{in}\left(1 - \sqrt{\frac{V_{in}}{V_0}}\right)}{2L_1 d'} \tag{15}$$

where V_0 is the average value of output voltage v_0 in steady-state.

It is clear that if the inductor current operates in sliding mode, the switching frequency of quadratic boost converter depends only of the input voltage. This is mainly due to the hysteresis band limits are fixed parameters, and the output voltage is regulated with zero error by means of the external control loop. On the other hand, with a non-ideal model the approach presented earlier is modified due the presence of the parasitic components. Assuming that inductor current $i_{L1}(t)$ is approximated by the first term of its Taylor development in order to exhibit a triangular shape waveform, expressions (13) and (14) become (16) and (17) respectively where it can be observed that the modification on the duration of on and off subintervals is due to the voltage drop in diodes D_2 and D_3 respectively.

$$t_{ON} = \frac{2L_1\delta}{V_{in} - V_{D2}} \tag{16}$$

$$t_{OFF} = \frac{-2L_1\delta}{V_{in} - V_{D3} - V_{C1}} \tag{17}$$

The surface in the figure 9 shows the behavior of the switching frequency in the converter as function of the input voltage and output power using the parameters of Table 1. It is worth to point out that the frequency variation along the input voltage range is significantly greater than the change along the output power range.

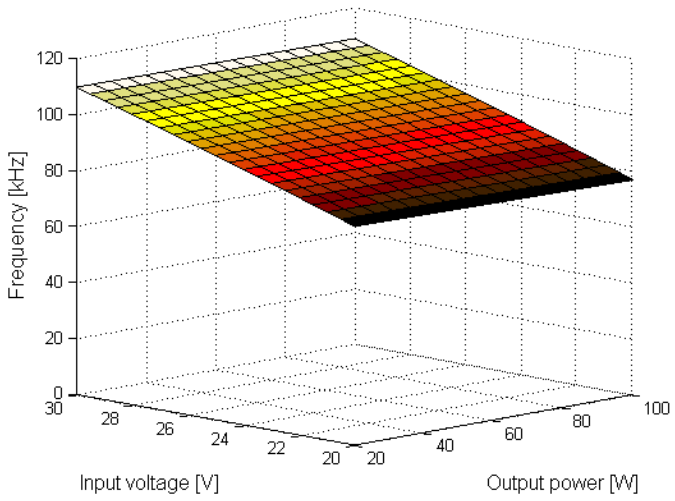

Fig. 9. Switching frequency as a function of load resistance and input voltage.

To verify the above mentioned results, figure 10 depicts the difference in switching frequency in two equilibrium points that has been measured in a 100 W laboratory prototype. In the upper oscilloscope capture the quadratic boost converter operates with an input voltage of 20.5Vdc and the measured switching period is 11.4μs, which corresponds approximately to a switching frequency of 87.7 kHz. In the

lower oscilloscope capture the converter operates with an input voltage of 30.4Vdc yielding a switching frequency of 100 kHz.

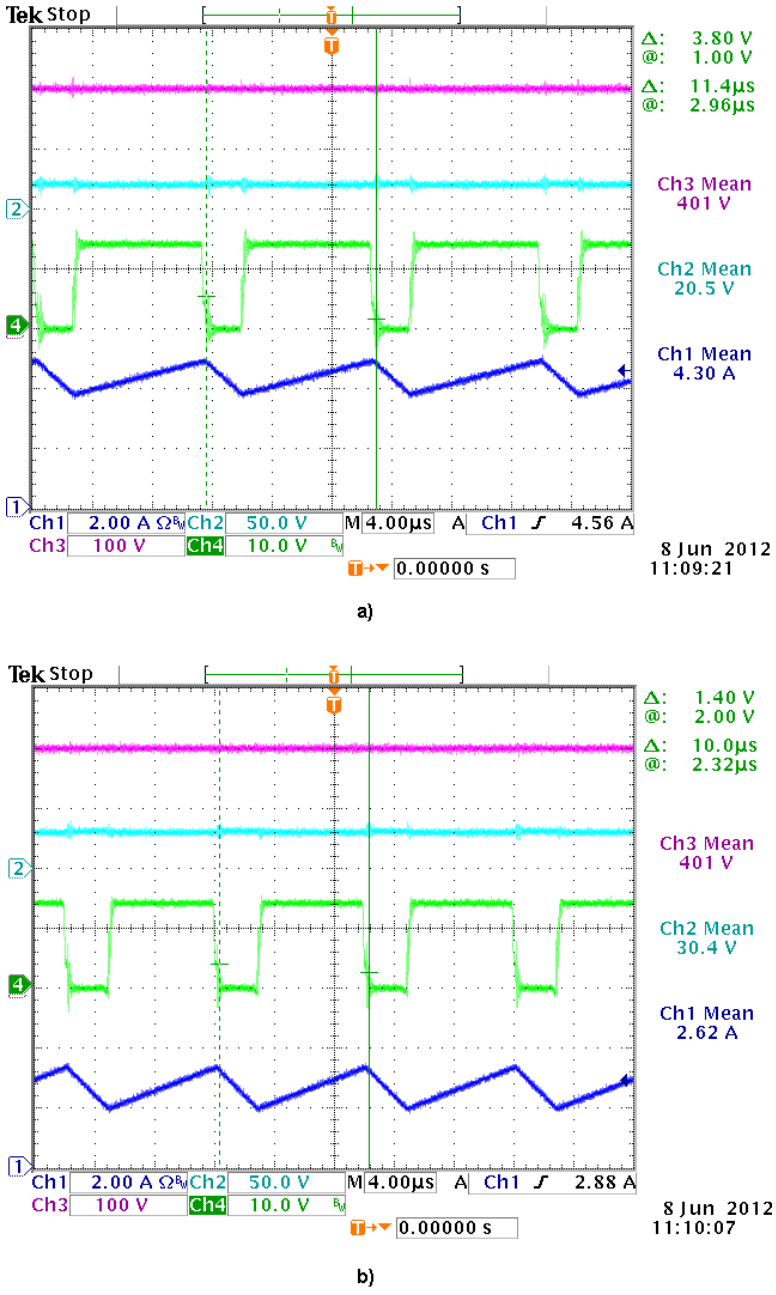

Fig. 10. Frequency variation for two different input voltage conditions for 80W: a) Vin=20V, b) Vin=30V.

4. EFFICIENCY ANALYSIS AND MEASUREMENTS

A complete efficiency analysis takes into account both conduction and switching losses [7], [14], [15], [16]. The conduction losses are produced by the DC and AC current components in the circuit. The switching losses mainly depend on the commutation characteristics of the power switches, namely, the switch voltage in OFF-state, the switch current in ON-state, and the switching frequency. In sliding-mode operation this analysis is not trivial due to the variation of the switching frequency and its dependence on both input voltage and current load. Hence, an algorithm in MATLAB has been developed in order to evaluate the efficiency of the converter for all steady-state operational conditions.

In order to calculate the converter efficiency in a fixed operating point, the algorithm requires the parameters of the complete model presented in section II. Additionally, a single evaluation requires the values of desired output voltage, input voltage, output power and amplitude of the hysteresis band. Our algorithm calculates the ideal duty cycle using (6) and increments this value until the output voltage reaches the desired value in the equation system (4). At this point, the algorithm has the mean values of the four state variables for the equilibrium point. In the next step, the algorithm generates the current signals and computes the RMS values and the conduction losses in each element based on the expressions of Table 2. It is worth to note that the AC components were not neglected what results in a more accurate approach. Finally, the algorithm computes the switching frequency and the switching losses using the expressions presented in Table 3 where the values $\overline{I_{L1}}$ and $\overline{I_{L2}}$ represent the mean values of the inductor currents, ΔI_{L2} is the amplitude of the current ripple in the inductor L2, t_r and t_f are the rise time and the fall time of the MOSFET, t_{rr} and Q_{rr} are the reverse recovery time of the diodes and the reverse recovery charge, respectively. The corresponding values of these parameters are presented in Table 4. Thus, the efficiency is obtained using the relation between input and output power of the converter. A reproduction

of this method along the operating ranges of input voltage and output power allows obtaining a 3D representation of the efficiency to facilitate the interpretation of its dependence on both variables.

Table 2. Expressions used in the reported MATLAB -based algorithm to compute the conduction losses

Type of Loss	Expression
Losses in inductors (Assuming 30% in core losses)	$P_L = 1.3 \cdot \left({I_{L_{RMS}}}^2 \cdot R_L \right)$
Losses in capacitors	$P_C = {I_{C_{RMS}}}^2 \cdot R_C$
Losses in the MOSFET	$P_{MOS} = {I_{M_{RMS}}}^2 \cdot R_{DSon}$
Losses in diodes	$P_D = {I_{D_{RMS}}}^2 \cdot R_D + \overline{I_D} \cdot V_D$

Table 3. Expressions used in the reported MATLAB- based algorithm to compute the switching losses

Loss Detail	Expression
ON transition losses	$P_{ON} = \left(\frac{1}{2} \left(\overline{I_{L1}} + \overline{I_{L2}} - \delta - \frac{1}{2} \Delta I_{L2} \right) \cdot \left(t_r + 2t_{rr} \right) + 2Q_{rr} \right) \cdot V_{C2} \cdot f_s$
OFF transition losses	$P_{OFF} = \frac{1}{2} \left(\overline{I_{L1}} + \overline{I_{L2}} + \delta + \frac{1}{2} \Delta I_{L2} \right) t_f \cdot V_{C2} \cdot f_s$
Gate charge losses	$P_{GATE} = \frac{1}{2} {V_{gate}}^2 \cdot C_{gate} \cdot f_s$

Table 4. Commutation parameters of the power semiconductors

Parameter	Value
t_r (STW45NM50)	23ns
t_f (STW45NM50)	35ns
V_{gate} (STW45NM50)	12V
C_{gate} (STW45NM50)	3.7nF
t_{rr} (MUR860)	30ns
Q_{rr} (MUR860)	50nC

Figure 11 shows the surface obtained with the algorithm that predicts the efficiency of the quadratic boost converter as a function of input voltage and output power taking into account the parameter values presented in Table 1 and Table 4. The converter operates with a PI-regulated output voltage external control loop and a sliding-mode internal control loop for the input-inductor current. It is possible to observe that the maximum efficiency is 84% whereas the minimum one is 75.2%. The better case corresponds to the maximum input voltage and maximum output power conditions while the worst case is obtained with the maximum input voltage and the minimum output power. It is worth to mention that when the converter delivers an output power higher than 35W, the efficiency within the complete range of the input voltage is always higher than 80%.

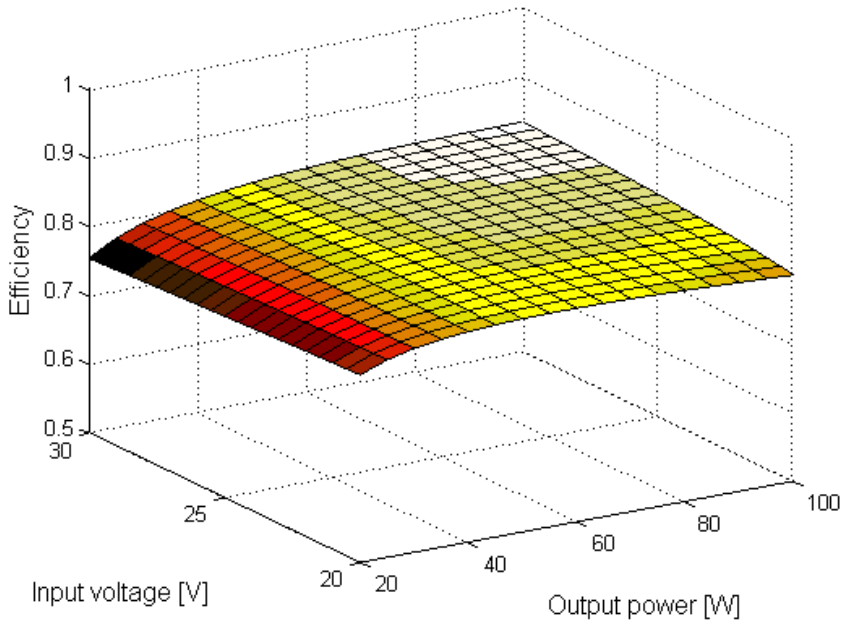

Fig. 11. Efficiency as a function of load resistance and input voltage.

When the input current operates in sliding-mode and the output voltage is regulated, a diminution in the input voltage induces an increment in the input current, and therefore an increment in the conduction losses. However, a diminution in the switching frequency is also produced. An interesting conclusion is that the diminution in the switching losses compensates the increment of conduction losses, and due to this fact, the converter efficiency in all operating conditions does not exhibit significant changes.

In order to verify the algorithm predictions, a 100W laboratory prototype has been designed to operate with input voltages between 20V and 30V. The practical circuit diagram with element values is illustrated in figure 12, a photograph of the prototype is shown in figure 13 and the workbench used in proofs and measurements is presented in figure 14. The equipment used is specified in Table 5. In the laboratory test, the converter has been operating in different equilibrium points by changing input voltage

and load. Figure 15 shows an oscilloscope capture with the signals of the state-variables specifying the mean values. If the values of the load resistance and input voltage are known, the CH4 signal (output voltage) will allow to calculate the output power while the CH1 signal (input current) will allow to obtain the input power.

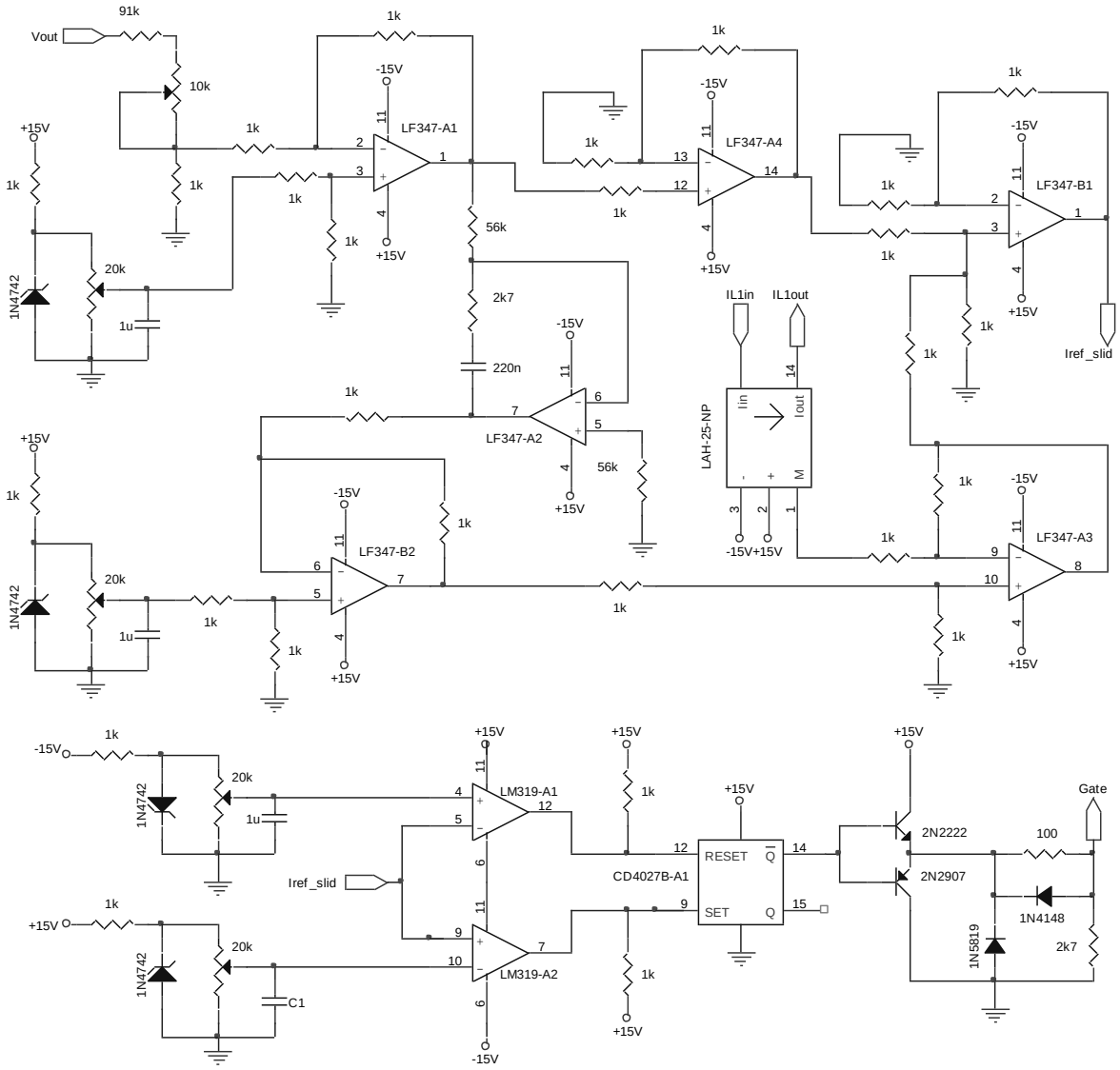

Fig. 12. Detail of the circuit implementation of the sliding-mode based controller.

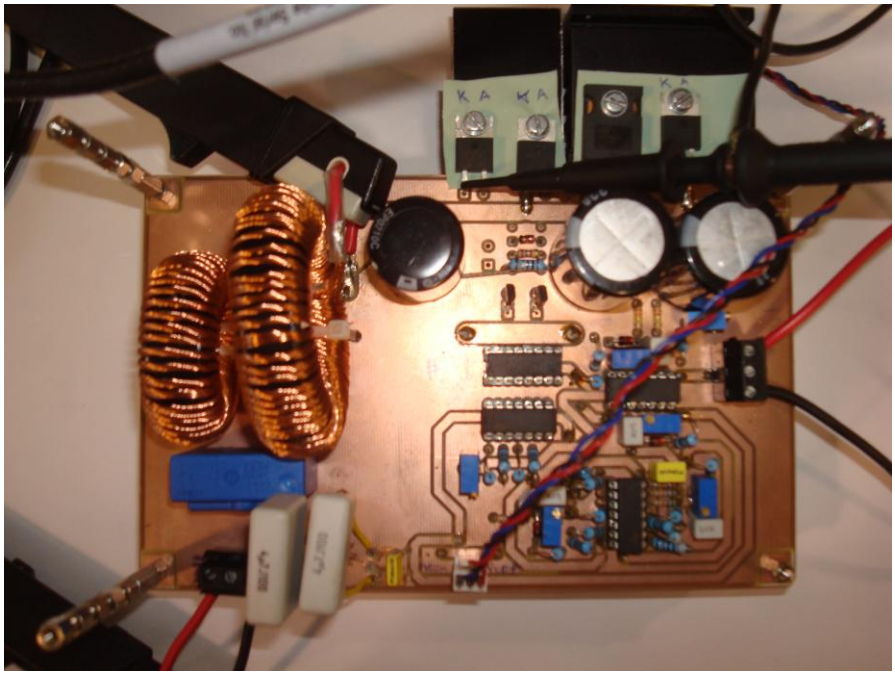

Fig. 13. Experimental prototype of a boost quadratic converter.

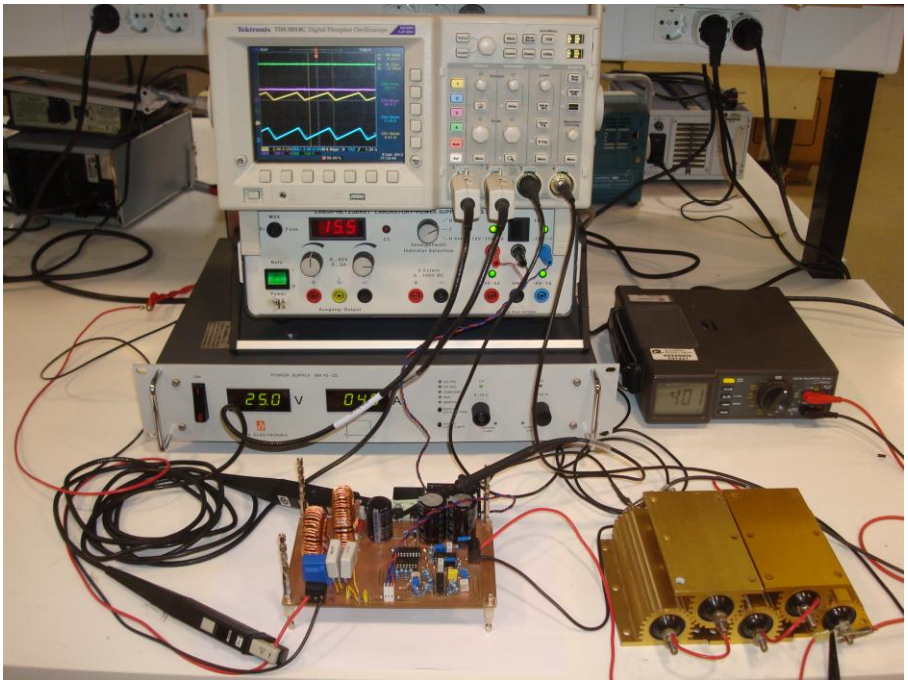

Fig. 14. Workbench for experimental measurements.

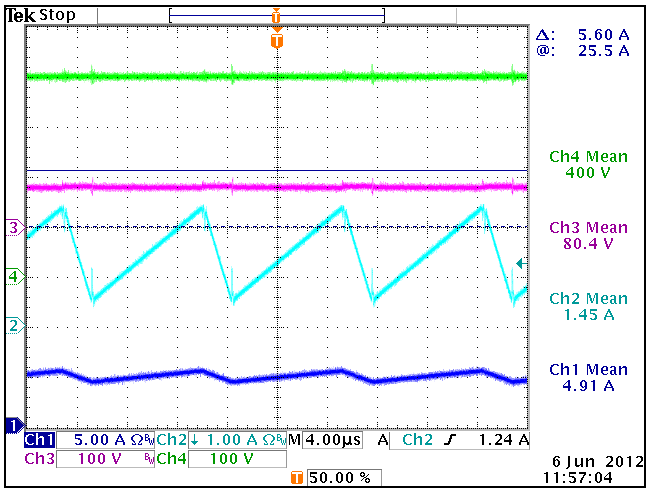

Fig. 15. Experimental waveforms of state variables for an equilibrium point.

Table 5. Workbench equipment used in the prototype measurements

Device	Reference
Power Supply control circuit	Elektro-Automatik EA-PS 2323A +/-15V
Power Supply power circuit	DELTA Electronica SM 70-22
Oscilloscope	TEKTRONIX TDS3014C Digital Phosphor
Current probes	TEKTRONIX TCP-202 Current probes
Multimeter	PROMAX DIGITAL MULTIMETER MD-200

Finally, figure 16 shows the surface obtained with the efficiency measurements made in the prototype in the whole operating range of both input voltage and output power. The maximum efficiency is 84.4% while the minimum one is 74.6%. The better case and the worst case correspond to the same conditions observed with the simulation results. Therefore, the measurements allow concluding that the

theoretical analysis and the reported algorithm for efficiency prediction are in good agreement with the experiments. At the same time, the results of efficiency evaluation demonstrate that a boost quadratic converter can be efficiently used within the ranges of voltage and power of transformer-less grid-connected PV micro- inverters.

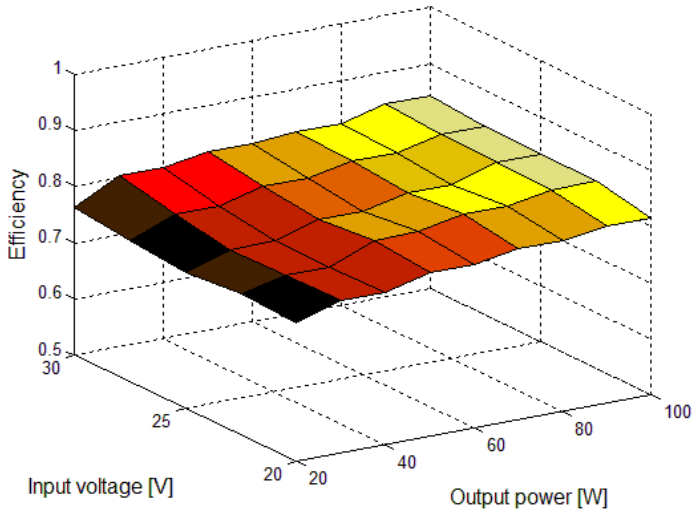

Fig. 16. Measured converter efficiency as a function of output power and input voltage.

5. CONCLUSIONS

This work has presented a complete efficiency analysis of the quadratic boost converter operating with a sliding-mode based control system. This analysis can be extended to any DC-DC switching converter with the same control system operating in CCM. The analysis has been supported with a MATLAB based algorithm that computes both conduction and switching losses with the aim to assess the efficiency along the converter operational range and takes into account the frequency variation due to the sliding-mode controller. The algorithm predictions are in good agreement with the experimental results.

The obtained results can be used to find the optimum set of parameters of the quadratic boost, i.e., selection of the switching frequency minimizing the switching losses and appropriate choice of

semiconductors with small series resistance or small forward voltage drop. Considering the potential application of the quadratic boost to achieve high-gain in the DC-DC stage of solar micro-inverters, a detailed study of its dynamic behaviour under sliding-mode control and the analysis of its operation in discontinuous conduction mode (DCM) are still open subjects whose solution could help engineers to better design this type of converters.

REFERENCES

[1] LM5046, SM72295. Application Note 2116. SolarMagic ICs in Micro-Inverter Applications, Literature Number: SNVA471A, National Semiconductor, 2011

[2] Maksimovic, D., and Cuk, S.: 'Switching Converters with wide DC conversion range'. IEEE Trans. Power Electron., 1991, 6, (1), pp. 151-157

[3] Matsuo, H., and Harada K.: 'The cascade connection of switching regulators'. IEEE Trans. Indust. Applic., 1976, 3, (2), pp 192-198

[4] Wai, R-J., and Duan, R-Y.: 'High step-up converter with coupled-inductor'. IEEE Trans. Power Electronics., 2005, 20, (5), pp. 1025-1035

[5] Wai, R-J., Lin C-Y., Duan, R-Y., and Chang, Y-R .: 'High efficiency DC-DC converter with high voltage gain and reduced switch stress'. IEEE Trans. Indust. Electron., 2007, 54, (1), pp. 354-364

[6] Abutbul, O., Gherlitz, A., Berkovich, Y., and Ioinovici A.: 'Step-up switching-mode converter with high voltage gain using a switched –capacitor circuit'. IEEE Trans. Circuits and Syst.-Part I, 2003, 50, (8), pp.1098-1102

[7] Walker, G.R., and Sernia, P.C.: 'Cascaded DC-DC converter connection of photovoltaic modules'. IEEE Trans. Power Electron., 2004, 19, (4), pp. 1130- 1139

[8] Ortiz-Lopez, M.G., Leyva-Ramos, J., Carbajal-Gutierrez, E.E., and Morales-Saladaña, J.A.: 'Modeling and analysis of switch –mode cascade converters with a single active switch'. IET Power Electron., 2008, 1, (4), pp. 478-487

[9] Utkin, V., Guldner, J. and Shi, J.: 'Sliding mode control in electromechanical systems' (CRC Press, 2nd edition, Taylor and Francis Group, 2009)

[10] Erickson, R.W., and Maksimovic, D.: ‘Fundamentals of power electronics’ (Kluwer Academic Publishers. 1999)

[11] Ortiz-Lopez, M.G., Leyva-Ramos, J., Diaz-Saldierna, L.H., Garcia-Ibarra, J.M., Carbajal-Gutierrez, E.E.: ‘Current-Mode Control for a Quadratic Boost Converter with a Single Switch’, Proc. Conf. IEEE Power Electron Spec. (PESC’07), 2007, pp.2652-2657

[12] Vidal-Idiarte, E., Martinez-Salamero, L., Guinjoan, F., Calvente, J., and Gomariz, S.: ‘Sliding and fuzzy control of a boost converter using an 8-bit microcontroller’, *IEE Proc-Electr. Power Appl.*, 151, (1), 2004

[13] Leyva-Ramos, J., Ortiz-Lopez, M.G., Diaz-Saldierna, L.H., and Morales-Sandaña, J.A.: ‘Switching regulator using a quadratic boost converter for wide DC conversion ratios’. IET Power Electron., 2009, 2, (5), pp. 605-613

[14] Ivanovic, Z., Blanusa, B., Knezic, M.: ‘Power Loss Model for Efficiency Improvement of Boost Converter’. Proc. XXIII International Symposium on Information, Communication and Automation Technologies (ICAT), 2011, pp. 1-6

[15] Eichhorn, T.: ‘Boost Converter Efficiency through Accurate Calculations’. Power Electronics Technology. Sep 2008, pp. 30-35,

[16] Boost converter has High Efficiency at Light Loads. Application Note 110. MAXIM, 1998